Relaxation of the mercury 6^3P_0 and 6^3P_1 states[a)]

M. Stock,[b)] E. W. Smith, R. E. Drullinger, and M. M. Hessel

Laser Physics Section, National Bureau of Standards, Boulder, Colorado 80302
(Received 26 April 1977)

The relaxation of 6^3P_0 mercury atoms excited by a laser pulse was measured for densities ranging from 2×10^{17} to 8×10^{18} cm^{-3}. The decay of the 253.7 nm resonance line was also measured for densities ranging from 5×10^{16} to 10^{18} cm^{-3}. The decay coefficients were analyzed to yield rate coefficients for three body molecular formation, the $^3P_1 \rightarrow {}^3P_0$ collision rate and a collisional quenching rate for the $^3P_0$ state. Small loss rates due to diffusion and radiation were also observed and found to be consistent with theoretical estimates of these quantities.

I. INTRODUCTION

The relaxation of the 6^3P states of the mercury atom is normally studied at low mercury densities (below 3×10^{16} cm^{-3}), where the 6^3P_1 state can be readily excited by absorption of the 253.7 nm resonance line.[1-3] At higher pressures the resonance line becomes optically thick and the exciting radiation is all absorbed in a thin sheath at the boundary of the containment cell, thus making both the experiments and the analysis very difficult.

In this paper we present a method for efficiently exciting the 6^3P_0 state by absorption of laser radiation in mercury molecules which quickly dissociate to form the 6^3P_0 atoms. Using this technique we have been able to study the relaxation of 6^3P_0 atoms at mercury densities ranging from 2×10^{17} to 8×10^{18} cm^{-3}. Methods are discussed for extending this density range.

We have also studied the decay of the $6^3P_1 - 6^1S_0$ resonance line at 253.7 nm. These fluorescence measurments were made at densities from 5×10^{16} to 10^{18} cm^{-3}.

The experimental data are analyzed in terms of a simple two level model for mercury atoms. Three body molecular formation rates the order of 1.6×10^{-31} cm^6 sec^{-1} were obtained for both the 6^3P_0 and 6^3P_1 states. A binary collision rate of 2.8×10^{-13} cm^3 sec^{-1} was obtained for $^3P_1 - {}^3P_0$ transitions and a rate of 4×10^{-14} cm^3 sec^{-1} was obtained for quenching of the $^3P_0$ state by binary collisions. Small effects due to diffusion and radiation were also observed and found to be in agreement with theoretical estimates.

II. EXPERIMENTAL PROCEDURE AND APPARATUS

The 6^3P_1 and 6^3P_0 atomic states are populated by optical pumping at 256 nm. This radiation is absorbed by mercury atom pairs (collision complex) to form Hg_2 excimers in high vibrational levels of the 1_u state (Fig. 1). Some of this excitation is converted directly into 6^3P_1 atoms since our pump wavelength lies within kT of the 253.7 nm resonance line ($6^1S_0 - 6^3P_1$). In addition, the rotational mixing of the 1_u state with the O_u^- state at small internuclear distances allows the bound 1_u molecules to dissociate into $6^1S_0 + 6^3P_0$ atoms, thus populating the 6^3P_0 state. Collisions can also produce vibrational relaxation of the excited 1_u state which will ultimately result in molecular radiation in the 335 nm band (Fig. 1) or in the 485 nm band which has been identified as mercury trimer emission.[4,5] By monitoring the molecular fluorescence as a function of time we find that over 90% of the pump laser excitation is converted into 6^3P atoms and, by monitoring the 6^3P_0 population with the probe laser discussed below, we find that over 90% of the 6^3P population resides in the 6^3P_0 state. This optical pumping scheme thus provides a very efficient method of producing 6^3P_0 metastables. We mention in passing that the decay of the molecular fluorescence at 256 nm was essentially coincident with our 5 nsec pump laser pulse for densities above 5×10^{17} cm^{-3}. This would indicate that the 1_u molecules are converted into $^3P_0$ atoms at a rate faster than 2×10^8 sec^{-1}, which greatly exceeds the radiative A value $A_{256} \simeq 10^7$ sec^{-1} found in Ref. 5.

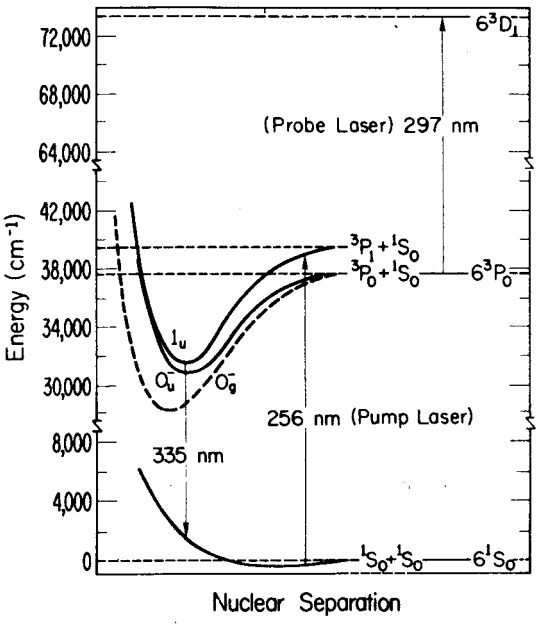

FIG. 1. Energy level diagram showing the 6^3P_0 and 6^3P_1 atomic states as well as some of the molecular states which dissociate to them. The pump and probe laser transitions are noted as well as the location of the center of the 335 nm molecular band which was used to monitor the molecular population.

a)Supported in part by ERDA Contract #E(49-1)-3800 and by ARPA Order #891, Amendment 11.

b)Postdoctoral Research Fellow supported by the Deutsche Forschungs Gemeinschaft. Present address: Universität Kaiserslautern, Fachbereich Physik, 675 Kaiserlautern, West Germany.

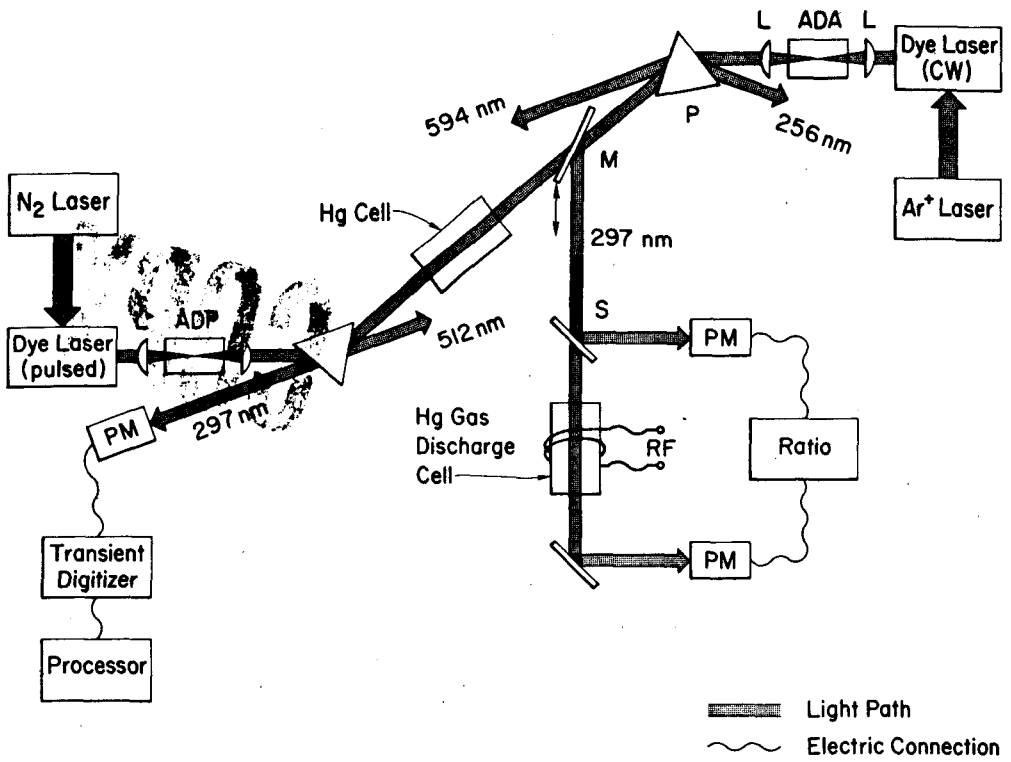

FIG. 2. Schematic diagram of the apparatus.

The pump laser, shown on the left side of Fig. 2, consisted of a commercial nitrogen laser (180 kW, 10 nsec pulse) which was used to pump a dye laser built in the Hänsch configuration[6,7] employing a dye cell, beam expanding telescope, grating for tuning wavelength, Glan-Thompson polarizer, and an end mirror with 40% transmission. Using a coumarin dye, the dye laser produced up to 50 kW at 512 nm with a spectral bandwidth of 0.03 nm and a pulse width of 10 nsec. The dye laser beam was then frequency doubled by a temperature tuned ADP crystal and the uv output was separated from the visible beam with a quartz prism. This 15 kW, 10 nsec, 256 nm laser pulse was used as the pump laser in Fig. 1.

The $6\,^3P_0$ population was monitored by the absorption of a probe laser tuned to the $6\,^3P_0$–$6\,^3D_1$ atomic transition at 296.7 nm (see Fig. 1). The probe laser, shown on the right side of Fig. 2, consisted of a commercial 15 W argon laser which pumps a jet stream dye laser with Rhodamine 6G dissolved in ethylene glycol; the output wavelength was selected with a three element birefringent filter. Using only 4 W of argon laser pump power (all lines) the dye laser produced 300 mW of output power at 593.4 nm in a spectral bandwidth the order of 0.005 nm. The dye laser beam was then frequency doubled in a temperature tuned ADA crystal, with an efficiency the order of 0.01%, and the resulting 296.7 nm laser beam was used as the probe laser in Fig. 1.

The sample cell was a quartz tube 5 cm long by 2 cm in diameter heated in a brick oven whose temperature was controlled to within a few hundredths of a degree. A small tube 4 mm in diameter was connected to the main cell body and extended vertically downward into a second oven which was also temperature controlled. This vertical tube served as a mercury reservoir. The upper and lower oven temperatures could be varied independently, thereby permitting independent control of both temperature and density. This type of oven system and the filling procedures which were used to insure high purity are described in more detail in Ref. 4.

To facilitate tuning the probe laser to the $6\,^3P_0$–$6\,^3D_1$ atomic absorption we employed a high frequency (rf) excited gas discharge which produced steady state $^3P_0$ densities the order of 10^{13} cm^{-3}. A moveable mirror M in Fig. 2 was used to deflect the probe laser beam into the discharge cell, where the atomic absorption was measured by comparing the signal seen by two photomultipliers (P.M.) which sampled the laser beam before and after passage through the discharge tube. The dye laser and ADA crystal were then adjusted to tune the probe laser to the maximum atomic absorption. With the probe laser thus tuned the mirror was removed and the beam was allowed to pass through the sample cell colinearly with the pump beam. After passage through the sample cell the probe beam was separated from the pump beam with a prism and directed to the transient recording system shown in Fig. 2. This recording system consisted of a photomultiplier to detect the transmitted probe intensity, a transient digitizer (eight bit, 2000 channel) with 10 nsec time resolution to record the transmission after each pump laser shot, a minicomputer to average subsequent shots, and a magnetic tape recorder to store the data for later analysis on a larger computer.

Figure 3 shows the transmitted probe laser intensity as a function of time for three different atom densities. The probe laser absorption was the order of 5% or less; thus there was a large dc component in the transmitted intensity which has been removed from these traces. Noise associated with this offset in fact limited the low-

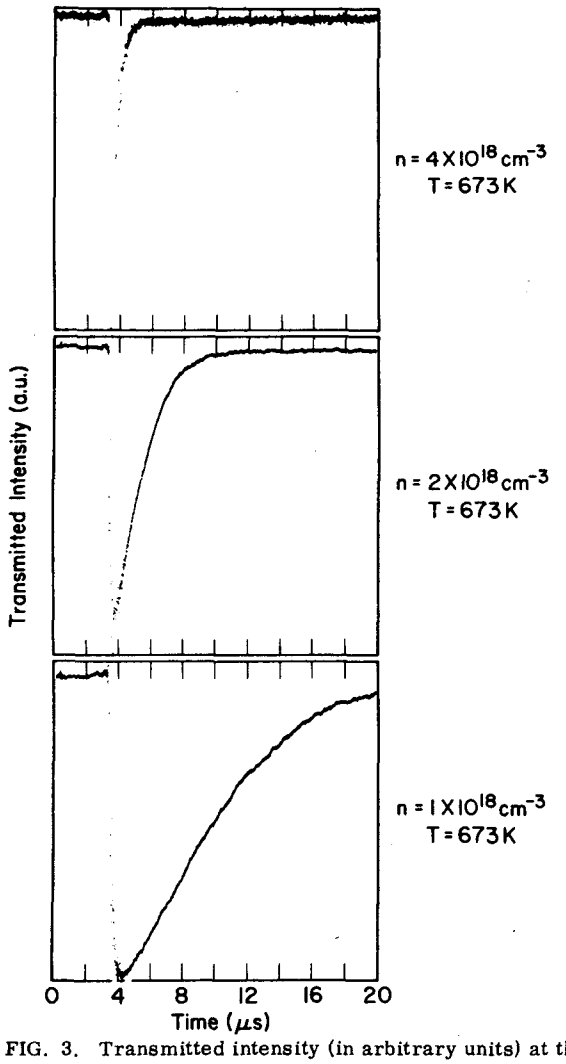

FIG. 3. Transmitted intensity (in arbitrary units) at the probe laser wavelength 297 nm as a function of time for three different densities. A large dc offset has been removed in order to show the absorption signal more clearly; the absorption never exceeded 5% of the transmitted intensity.

est density at which we could measure the $^3P_0$ population.

This excitation technique could be extended to lower densities by construction of a longer sample cell; however, it must be noted that diffusion losses will then become important as $^3P_0$ atoms can migrate out of our 2 mm laser beam at densities less than 3×10^{17} cm^{-3}. Thus, at lower densities it will be desirable to use a beam expanding telescope for the laser beams. This would result in a loss of sensitivity which could be partially offset by tuning the pump laser closer to the 253.7 nm resonance line, thus increasing the absorption.

In addition to these $6\,^3P_0$ probe measurements, fluorescence measurements were also made by tuning the pump laser closer to the 253.7 nm resonance line to enhance absorption by the $6\,^3P_1$ state. The decay of the 253.7 nm line was then monitored as a function of time.

III. ANALYSIS OF $6\,^3P$ DECAY

A. General approach

In this paper we are interested in experiments in which the $6\,^3P_1$ and $6\,^3P_0$ levels are optically excited at temperatures the order of 673 K. We will therefore ignore the $6\,^3P_2$ states which lie 4620 cm^{-1} above the $6\,^3P_1$ level and consider only the $6\,^3P_0$ and $6\,^3P_1$ levels. In the Appendix we outline the mathematical details of our model for the decay of these two coupled levels and we find that the $^3P_0$ density is described by a function of the form

$$I = I_s e^{-\gamma_s t} - I_f e^{-\gamma_f t}, \tag{3.1}$$

where $\gamma_f > \gamma_s$ and $I_f < I_s$. The decay coefficients for the fast and slow decay components are given by,

$$\gamma_f = \beta + (\gamma_d^1/n) + nk_{01} + n^2 k_3^1 \tag{3.2}$$

$$\gamma_s = \beta[nk_{10}/(\beta + nk_{01})]\, e^{-\Delta E/kT} + (\gamma_d^0/n) + nk_q^0 + n^2 k_3^0, \tag{3.3}$$

where n is the gas density, β is the $^3P_1$ radiative loss rate (including the effect of radiation trapping[8], k_3^0 and k_3^1 are three body molecular formation rates from $^3P_0$ and $^3P_1$, respectively, $\Delta E = 1690$ cm^{-1} is the energy separation of the $^3P_0$ and $^3P_1$ levels, the binary collision rate coefficients for $^3P_0 \rightarrow {}^3P_1$ and $^3P_1 \rightarrow {}^3P_0$ are k_{10} exp $(-\Delta E/kT)$ and k_{01} ($k_{10} = 3k_{01}$ due to the threefold degeneracy of the $^3P_1$ level), γ_d^0/n and γ_d^1/n represent a simple approximation to diffusion losses, k_q^0 represents quenching of the $^3P_0$ level by binary collisions, and a similar term k_q^1 for the $^3P_1$ level was neglected since it is assumed to be much smaller than k_{01}.

Since the absorption of the probe laser never exceeds 5%, this absorption signal should be directly proportional to the $^3P_0$ atom density [i.e., Eq. (3.1)]. We may therefore obtain both fast and slow decay coefficients from a semilog plot of the absorption signal versus time such as Fig. 4. In data such as this the fast component was obtained by back extrapolating the slow component and subtracting the observed decay curve from it. The

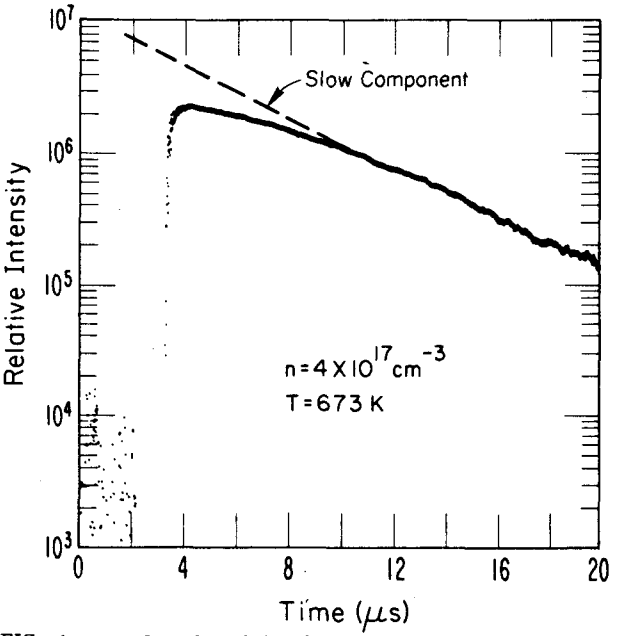

FIG. 4. Semilog plot of the absorption signal as a function of time illustrating the fast decay component which is seen at early times. This component is obtained by back extrapolating the slow component (dashed line) and subtracting the observed decay signal.

fast component could then be plotted separately, thereby permitting a determination of both γ_f and γ_s.

At high densities ($n > 10^{18}$ cm^{-3}) a third decay component could be seen at very late times as shown in Fig. 5. The decay coefficient for this component was found to be identical to the known decay coefficient for mercury molecular fluorescence[3,4]; hence, it is ascribed to back rates from the molecules. That is, at higher densities the $6\,^3P_0$ atoms decay primarily by forming molecules and, after a few microseconds, the molecular population builds up to the point where the back rate (molecules – atoms) establishes a dynamic balance between the atomic and molecular populations. After this point the system (atoms plus molecules) decays together at the molecular decay rate since that is the slowest loss rate. This phenomenon does not occur at lower densities because both the back rates and the molecular formation rate are much slower. At the late times and high densities where this molecular decay component is observed, the $^3P_0$ and $^3P_1$ states have already come into equilibrium with one another and are decaying together at the slower atomic decay rate γ_s. We may therefore adopt a simple model consisting of two species, atoms and molecules. In this model the atomic decay is given by the usual sum of two exponentials $I_a \exp(-\gamma_s t) + I_m \exp(-\gamma_m t)$ where γ_s is the slow atomic decay rate and γ_m is the molecular decay rate. This functional form was used to separate the atomic and molecular decay coefficients for cases such as that shown in Fig. 5.

The fast and slow atomic decay coefficients obtained from the $^3P_0$ decay measurements are plotted as a function of gas density in Fig. 6. The fast decay coefficient could not be evaluated by this method for very low densities because its amplitude became too weak.

At very high densities the fast component was observable only for very short times and the uncertainties resulting from the subtraction of the measured decay from the back-extrapolated slow decay component became excessive.

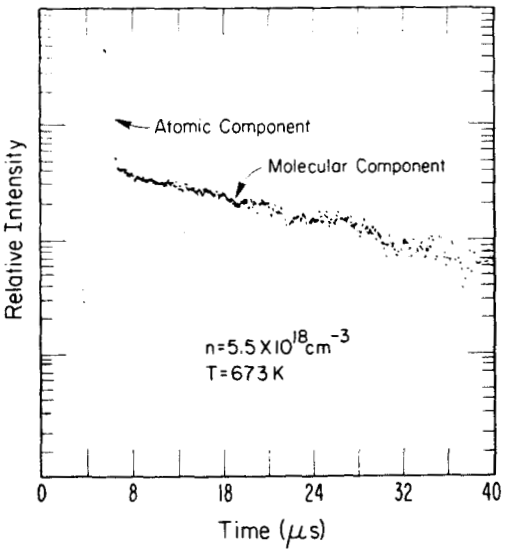

FIG. 5. Semilog plot of the absorption signal as a function of time illustrating the molecular decay component. The molecular decay component was seen at late times for densities above 10^{18} cm^{-3}.

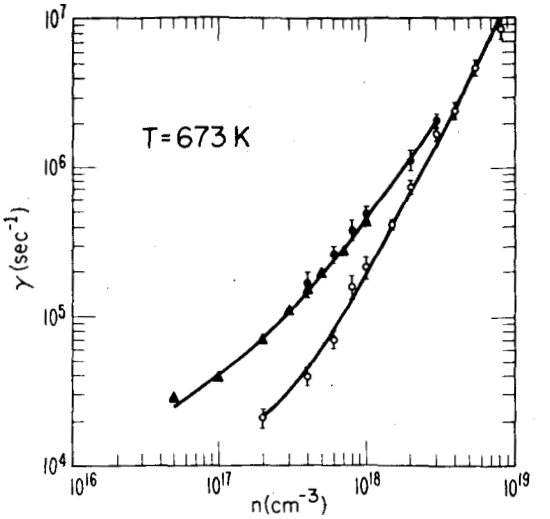

FIG. 6. Fast and slow atomic decay coefficients as a function of density at a fixed temperature of 673 K. The open circles denote measurements of the slow decay coefficient by monitoring the decay of the $^3P_0$ state. The solid circles denote the fast decay coefficient as obtained from the $^3P_0$ decay measurements. The solid triangles denote measurements of the fast decay coefficient obtained from the decay of the 253.7 nm fluorescence. The solid curves show our fits to the experimental data using the parameters of Eqs. (3.2) and (3.3).

In addition to the $^3P_0$ decay measurements discussed above we also measured the decay of the 253.7 nm $6\,^3P_1 - 6\,^1S_0$ resonance line. This line also decayed as the sum of two exponentials governed by the fast and slow decay rates γ_f and γ_s. For densities greater than 2×10^{17} cm^{-3} the slow decay rate γ_s was treated as known (from the $^3P_0$ decay measurements) in order to reduce the number of parameters used in fitting the data. For densities below 2×10^{17}, the amplitude of the slow component was too weak to be seen. These fluorescence measurements were therefore used only to determine γ_f. The values of γ_f thus obtained are also plotted in Fig. 6.

The data for the fast decay coefficient were numerically fit to the function given in Eq. (3.2). This fit gave

$$k_3^1 = 1.65\times10^{-31}\ \text{cm}^6\ \text{sec}^{-1}, \tag{3.4}$$

$$k_{01} = 2.8\times10^{-13}\ \text{cm}^3\ \text{sec}^{-1}, \tag{3.5}$$

$$\gamma_d^1 \lesssim 10^{20}\ \text{cm}^{-3}\ \text{sec}^{-1}, \tag{3.6}$$

$$\beta \simeq 1.2\times10^4\ \text{sec}^{-1}. \tag{3.7}$$

We then treated k_{01} as known and, using $k_{10} = 3k_{01}$, the data for the slow decay coefficient were numerically fit to the function given in Eq. (3.3) resulting in

$$k_3^0 = 1.55\times10^{-31}\ \text{cm}^6\ \text{sec}^{-1}, \tag{3.8}$$

$$k_q^0 = 4\times10^{-14}\ \text{cm}^3\ \text{sec}^{-1}, \tag{3.9}$$

$$\gamma_d^0 = 1.04\times10^{21}\ \text{cm}^{-3}\ \text{sec}^{-1}, \tag{3.10}$$

$$\beta \simeq 10^4\ \text{sec}^{-1}. \tag{3.11}$$

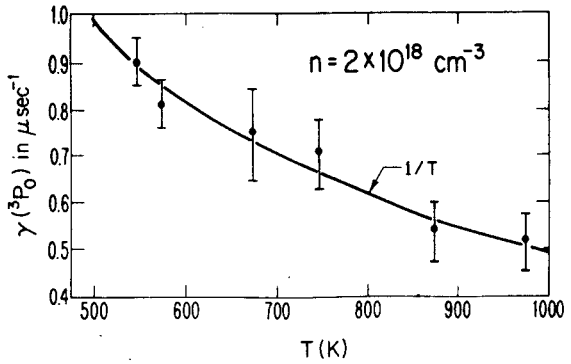

FIG. 7. Temperature dependence of the slow decay coefficient at a density of 2×10^{-18} cm^{-3}. At this density three body processes account for about 90% of the observed decay; hence, this temperature dependence can be ascribed to the three body molecular formation rate. The solid curve shows a $1/T$ fit to the experimental data.

The least squares fit to the data determines the termolecular rates k_3^0 and k_3^1 and the binary rates k_{01} and k_q^0 to within about 10%. The radiative rate β and the diffusion coefficients γ_d^1 and γ_d^0 are much less accurate due to the lack of low density data. The coefficient γ_d^0 is accurate to within about 50%, β is accurate only to within an order of magnitude and we could only obtain an upper bound for the value of γ_d^1. These error estimates are based on the accuracy of our numerical fit to the data; systematic errors in the data could introduce errors of unknown magnitude. The error bars in Fig. 6 illustrate the reproducibility of our measurements. Each of these rates will be discussed in more detail in the following sections

B. Three body molecular formation rates

Our rate coefficient k_3^0 for three body molecular formation from the $^3P_0$ state is somewhat smaller than the value 10^{-30} cm^6 sec^{-1} obtained by McCoubrey[3]; however, the latter experiments were done at much lower densities ($n \leq 3\times10^{16}$ cm^{-3}) where molecular formation is not the dominant decay process. Consequently our value is likely to be more accurate.

It is interesting to compare our three body rate with the corresponding rate in mercury–nitrogen mixtures. The latter has been measured by several authors[9–11] and ranges from 10^{-30} to 16×10^{-30} cm^6 sec^{-1}, which are between one and two orders of magnitude larger than our rate for pure mercury. It is usually assumed that Hg_2 (1_u) is formed by a two step process[12]

$$\begin{aligned} &Hg(^3P_0) + Hg(^1S_0) - Hg_2^*, \\ &Hg_2^* + M - Hg_2(1_u) + M, \end{aligned} \qquad (3.12)$$

in which the quasimolecule Hg_2^* is stabilized by collision with a particle M [N_2 in the case of the mercury–nitrogen experiments or $Hg(^1S_0)$ in our case]. This model would seem to imply that N_2 is one or two orders of magnitude more effective than $Hg(^1S_0)$ in stabilizing the quasimolecule Hg_2^*, perhaps due to the fact that it can take up some energy in its internal states (i.e., rotation–vibration).

The temperature dependence of the $^3P_0$ decay coefficient at a density of 2×10^{18} cm^{-3} is shown in Fig. 7. At this density the three body rate is about an order of magnitude greater than the other processes; hence, this temperature dependence can be ascribed to k_3^0. A slow decrease in k_3^0 with increasing temperature is observed similar to that found in other atomic recombination processes.[13]

The rate coefficients k_3^0 and k_3^1, for three body molecular formation from the $^3P_0$ and $^3P_1$ states were found to be essentially equal. We also note in passing that k_3^1 represents the loss of $^3P_1$ atoms due to molecular formation by three body recombination. These molecules could be formed in highly excited vibrational states which dissociate (either collisionally or spontaneously) to form $^3P_0$ atoms before they are vibrationally relaxed to form stable molecules. An indication that this may occur is found in the general observation[10] that one does not see any appreciable molecular fluorescence until after a sizeable $^3P_0$ population is formed. In Sec. II we also noted that the high vibrational levels of the 1_u state, excited by our pump laser, dissociate very quickly to form $^3P_0$ atoms.

C. Two body loss processes

Our $^3P_1 - {}^3P_0$ rate coefficient, $k_{01} \simeq 2.8\times10^{-13}$ cm^3 sec^{-1}, is consistent with the results reported by Waddell and Hurst[14]; their cross sections range from 3×10^{-18} to 10^{-17} cm^2, corresponding to rates ranging from 9×10^{-14} to 3×10^{-13} cm^3 sec^{-1}. We have assumed that collisional quenching of the $^3P_1$ state, by transitions to the $6\,^1S_0$ ground state or the $6\,^3P_2$ state, is much slower than this $^3P_1 - {}^3P_0$ rate.

The binary collision rate for quenching of the $^3P_0$ state is $k_q^0 = 4\times10^{-14}$ cm^3 sec^{-1}. This quenching could be due to collision induced transitions directly to the $6\,^1S_0$ ground state or it could result from collision induced radiation. Collision induced radiation could occur during a collision in which the $6\,^3P_0$ and $6\,^1S_0$ atoms approach one another along the O_u^- molecular potential curve (see Fig. 1) making a collisional transition to the 1_u curve at small internuclear distances, thus becoming quasibound in the 1_u state. This quasibound molecule could radiate in the vicinity of 265 nm, thereby serving as a two body loss mechanism for the $^3P_0$ state. Mercury vapor is known to emit a molecular band at 265 nm which appears only at lower densities[15,16] where the 1_u radiative rate can compete more favorably with collisional stabilization. A similar quenching process could also be proposed in which quasibound *gerade* states are formed which relax via infrared radiative transitions to the 1_u state (as yet unobserved). It is not possible to distinguish between these different quenching processes with our present experimental data; thus our $k_q^0 = 4\times10^{-14}$ cm^3 sec^{-1} corresponds to a quenching cross section of 10^{-18} cm^2, which represents the combined effect of all two body quenching processes. This cross section compares favorably with cross sections for quenching of the $^3P_0$ state by collisions with molecules[17] which range from 10^{-18} to 10^{-16} cm^2.

It should be noted that a cross section for collisional quenching of $6\,^3P_0$ by $6\,^1S_0$ atoms is given by Massey[17] in Table 18.4 as 24×10^{-16} cm^2. This value was obtained

by Callear and Williams[18] using a mercury–nitrogen mixture, by plotting the $6\,^3P_0$ quenching rate as a function of N_2 density and assigning its value in the zero density limit to quenching by mercury atoms. Without measuring the mercury density dependence it would be very dangerous to take this value as a bimolecular quenching rate since $6\,^3P_0$ losses at low pressures are strongly affected by radiative and diffusion losses as well as small impurity concentrations. Callear and Mc Gurk[19] have in fact repeated the experiment of Callear and Williams[18] using an improved light source and obtained much higher $^3P_0$ quenching rates with N_2 as a collision partner. In this more recent work no attempt was made to estimate the corresponding rate using $Hg(^1S_0)$ as a collision partner. Thus the older value reported by Callear and Williams and by Massey should probably be disregarded.

D. Diffusion and radiation losses

The radiation and diffusion loss terms in Eqs. (3.2) and (3.3) make a very small contribution to the decay rates at the densities considered in this paper. Consequently these parameters are poorly determined by our experimental data. The values obtained are nonetheless consistent with theoretical predictions as we will show.

In order to calculate the diffusion coefficient γ_d^0 for the $^3P_0$ state we first note that our geometry is determined by the size of our pump and probe laser beams, i.e., if a $^3P_0$ atom diffuses out of the probe laser beam, it appears as a loss. Our system is thus a cylinder 5 cm long by 2 mm in diameter (the laser beam diameter). The diffusion coefficient for our temperature (673 K), obtained by scaling the 623 K results of Penkin and Redko[20] as $\sqrt{T}$, is $nD = 2.0\times10^{18}$ cm^{-1} sec^{-1}. The usual expression for the loss rate in a cylinder of radius R and length L is [see Eq. (8) of Ref. 3].

$$\gamma_d^0 = nD\left[(2.4/R)^2 + (\pi/L)^2\right]$$

$$= 1.1\times10^{21}\ \text{cm}^{-3}\,\text{sec}^{-1}. \qquad (3.13)$$

This agrees surprisingly well with our measured value 1.04×10^{21} cm^{-3} sec^{-1} given in Eq. (3.10).

Our data on the fast decay component could not be used to evaluate the $^3P_1$ diffusion coefficient γ_d^1. We were only able to estimate an upper bound the order of 10^{20} cm^{-3} sec^{-1}. This too is consistent with the experimental results of Phelps and McCoubrey,[21] which gave an upper limit for the $^3P_1$ diffusion coefficient somewhat smaller than that for the $^3P_0$ state; their theoretical arguments indicate that it may be about two orders of magnitude smaller.

The radiative loss rate β for the $^3P_1$ state may be calculated using the theory of Walsh[8] which includes the effect of radiation trapping. For a cylindrical geometry with a 2 mm diameter at a density of 2×10^{17} cm^{-3} we obtain $\beta \simeq 2.8\times10^4$ sec^{-1}. This value agrees reasonably well with the values 1.2×10^4 and 1.0×10^4 sec^{-1} obtained by fitting the fast and slow decay components.

APPENDIX. DECAY OF TWO COUPLED STATES

In this Appendix we will outline the mathematical details of our model for the decay of the $6\,^3P_1$ and $6\,^3P_0$ states. The $6\,^3P_0$ and $6\,^3P_1$ populations $n_0(t)$ and $n_1(t)$, are described by two coupled equations

$$\dot{n}_1(t) = -\Gamma_1 n_1(t) + \Gamma_{10} n_0(t), \qquad (A1)$$

$$\dot{n}_0(t) = -\Gamma_0 n_0(t) + \Gamma_{01} n_1(t), \qquad (A2)$$

where Γ_0 and Γ_1 represent the $6\,^3P_0$ and $6\,^3P_1$ loss rates and Γ_{10} and Γ_{01} represent the collisional coupling of these two states, respectively. This pair of equations has the solution

$$n_1(t) = A_1 e^{-\gamma_f t} + B_1 e^{-\gamma_s t}, \qquad (A3)$$

$$n_0(t) = A_0 e^{-\gamma_f t} + B_0 e^{-\gamma_s t}, \qquad (A4)$$

where

$$A_1 = \left[(\Gamma_1 - \gamma_s)\, n_1(0) - \Gamma_{10} n_0(0)\right]/(\gamma_f - \gamma_s), \qquad (A5)$$

$$B_1 = \left[(\gamma_f - \Gamma_1)\, n_1(0) + \Gamma_{10} n_0(0)\right]/(\gamma_f - \gamma_s), \qquad (A6)$$

$$A_0 = \left[(\Gamma_0 - \gamma_s)\, n_0(0) - \Gamma_{01} n_1(0)\right]/(\gamma_f - \gamma_s), \qquad (A7)$$

$$B_0 = \left[(\gamma_f - \Gamma_0)\, n_0(0) + \Gamma_{01} n_1(0)\right]/(\gamma_f - \gamma_s), \qquad (A8)$$

and the decay rates are given by

$$\left\{\begin{matrix}\gamma_f \\ \gamma_s\end{matrix}\right\} = \frac{\Gamma_1 + \Gamma_0}{2} \pm \tfrac{1}{2}\sqrt{(\Gamma_1 - \Gamma_0)^2 + 4\Gamma_{10}\Gamma_{01}}\,. \qquad (A9)$$

The loss rates and coupling terms for the $^3P_0$ and $^3P_1$ states are given by

$$\Gamma_0 = \frac{\gamma_d^0}{n} + n\,k_q^0 + n^2 k_3^0 + n\,k_{10}\,e^{-\Delta E/kT}, \qquad (A10)$$

$$\Gamma_1 = \beta + \frac{\gamma_d^1}{n} + n\,k_q^1 + n^2 k_3^1 + n k_{01}, \qquad (A11)$$

$$\Gamma_{01} = n\,k_{01} + n^2 f^1 k_3^1, \qquad (A12)$$

$$\Gamma_{10} = n\,k_{10}\,e^{-\Delta E/kT} + n^2 f^0 k_3^0\, e^{-\Delta E/kT}, \qquad (A13)$$

where n is the gas density, β is the $^3\Gamma_1$ radiative loss rate (which includes the effect of radiation trapping[8], k_3^0 and k_3^1 represent three body loss rates for the $^3P_0$ and $^3P_1$ states, k_q^0 and k_q^1 represent collisional quenching of $^3P_0$ and $^3P_1$, γ_d^0/n and γ_d^1/n represent a simple approximation to the diffusion losses of $^3P_0$ and $^3P_1$, k_{01} and $k_{10}\exp(-\Delta E/kT)$ represent the $^3P_1 \rightarrow {}^3P_0$ and $^3P_0 \rightarrow {}^3P_1$ binary collision rates ($k_{10} = {}^3k_{01}$ due to the threefold degeneracy of the $^3P_1$ level), and $\Delta E = 1690$ cm^{-1} is the energy spacing between $^3P_0$ and $^3P_1$.

The three body loss rates k_3^0 and k_3^1 result from the formation of vibrationally excited diatomic molecules. In Sec. II it was noted that highly excited 1_u molecules can decay rapidly into $6\,^3P_0$ atoms (faster than 10^8 sec^{-1} for densities above 5×10^{17} cm^{-3}). We must therefore allow for the possibility that some of the molecules formed via three body recombination of $6\,^3P_1 + 6\,^1S_0$ atoms may dissociate to form $6\,^3P_0 + 6\,^1S_0$ atoms before they can be collisionally relaxed to form stable diatomic molecules. This results in a three body mechanism for $^3P_0 \rightarrow {}^3P_1$ transitions which may dominate the normal binary collision process at high densities. The branching ratio f^1 represents the fraction of molecules formed by the three body process $n^2 k_3^1$ which dissociate to form $6\,^3P_0 + 6\,^1S_0$ atoms before they can be vibrationally relaxed to

form stable molecules. Similarly, the term $f^0 \exp(-\Delta E/kT)$ represents the fraction of excited molecules formed from $^3P_0$ atoms which dissociate to $^3P_1$ atoms before being vibrationally stabilized. The latter term insures that the population ratio n_1/n_0 will remain proportional to the Boltzmann factor $\exp(-\Delta E/kT)$ even if the three body mixing of $^3P_0$ and $^3P_1$ states should dominate over the two body process.

We will assume that the three body rate k_3^1 is the order of k_3^0; our analysis of the fast decay component in Sec. III will confirm this assumption. It is thus clear that $\Gamma_1 \gtrsim \Gamma_0$ and $\Gamma_1^2 \gg 4\Gamma_{01}\Gamma_{10}$. We may therefore evaluate the fast and slow decay rates γ_f and γ_s by series expanding the square root in Eq. (A9) in powers of $1/\Gamma_1^2$. To first order this procedure gives

$$\gamma_f \simeq \Gamma_1 + \frac{\Gamma_{10}\Gamma_{01}}{\Gamma_1} \simeq \beta + \frac{\gamma_d^1}{n} + n^2 k_3^1 + n k_{01}, \tag{A14}$$

$$\begin{aligned}\gamma_s &\simeq \Gamma_0 - \frac{\Gamma_{10}\Gamma_{01}}{\Gamma_1} \\ &\simeq \left(\frac{\Gamma_1 - nk_{01}}{\Gamma_1}\right) nk_{10}\, e^{-\Delta E/kT} + \frac{\gamma_d^0}{n} + n k_q^0 + n^2 k_3^0 \\ &\simeq \beta\left(\frac{n k_{10}}{\beta + nk_{01}}\right) e^{-\Delta E/kT} + \frac{\gamma_d^0}{n} + n k_q^0 + n^2 k_3^0,\end{aligned} \tag{A15}$$

where we have neglected terms of order $nk_{10}\exp(-\Delta E/kT)/\Gamma_1$ compared with unity and assumed that $k_{01} \gg k_q^1$. In Eq. (A15) the term $(\Gamma_1 - n k_{01})/\Gamma_1$ has been replaced by its value when $\beta + n k_{01} > n^2 k_3^1$ (also using[21] $\gamma_d^0 < \gamma_d^1$) since this term is negligible compared with $n^2 k_3^0$ when $\beta + nk_{01} < n^2 k_3^1$.

We evaluate Eq. (A7) and (A8) in the same manner and obtain

$$n^0(t) \simeq \left[n_0(0) - \frac{\Gamma_{01} n_1(0)}{\Gamma_1 - \Gamma_0}\right] e^{-\gamma_s t} - \left[\frac{\Gamma_{01} n_1(0)}{\Gamma_1 - \Gamma_0}\right] e^{-\gamma_f t}, \tag{A16}$$

which contains contributions from both fast and slow decay components. For the experiments discussed in this paper the amplitude of the slow decay component is greater than that of the fast component. Nonetheless, the latter was observable at early times for all the data analyzed and in many cases it was desirable to separate the fast and slow components using the functional form of Eq. (A16).

[1] M. Zemansky, Phys. Rev. **29**, 513 (1927).
[2] D. Alpert, A. O. McCoubrey, and T. Holstein, Phys. Rev. **76**, 1257 (1949).
[3] A. O. McCoubrey, Phys. Rev. **93**, 1249 (1954).
[4] R. E. Drullinger, M. M. Hessel, and E. W. Smith, Natl. Bur. Stand. Monogr. **143** (1975).
[5] E. W. Smith, R. E. Drullinger, M. M. Hessel, and J. Cooper, J. Chem. Phys. **66**, 5667 (1977).
[6] T. W. Hansch, Appl. Opt. **11**, 895 (1972).
[7] F. P. Schafer, *Topics in Applied Physics, Vol.* I, *Dye Lasers* (Springer, New York, 1973), p. 40.
[8] P. J. Walsh, Phys. Rev. **116**, 511 (1959).
[9] J. M. Campbell, S. Penzes, H. S. Sandhu, and O. P. Strausz, Int. J. Chem. Kinet. **3**, 175 (1971).
[10] S. Penzes, H. E. Gunning, and O. P. Strausz, J. Chem. Phys. **47**, 4869 (1967).
[11] R. A. Phaneuf, J. Skonieczny, and L. Krause, Phys. Rev. A **8**, 2980 (1973).
[12] J. Skonieczny, Acta Phys. Pol. A **49**, 807 (1976).
[13] V. N. Kondrat'ev, *Chemical Kinetics of Gas Reactions* (Pergamon, Addison-Wesley, 1964), p. 336.
[14] B. V. Waddell and G. S. Hurst, J. Chem. Phys. **53**, 3892 (1970).
[15] C. G. Matland and A. O. McCoubrey (unpublished data).
[16] R. E. Drullinger, M. M. Hessel, and E. W. Smith, J. Chem. Phys. **66**, 5656 (1977).
[17] H. S. W. Massey, *Electronic and Ionic Impact Phenomena* (Clarendon, Oxford, 1971), Vol. III, pp. 1693 and 1741.
[18] A. B. Callear and G. J. Williams, Trans. Faraday Soc. **60**, 2158 (1964).
[19] A. B. Callear and J. C. McGurk, Chem. Phys. Lett. **6**, 417 (1970).
[20] N. P. Penkin and T. P. Redko, Opt. Spectrosc. **36**, 132 (1974).
[21] A. V. Phelps and A. O. McCoubrey, Phys. Rev. **118**, 1561 (1960).